INORGANIC CHEMISTRY FRONTIERS

RESEARCH ARTICLE

View Article Online
View Journal | View Issue

Cite this: *Inorg. Chem. Front.*, 2025, **12**, 1176

Solvent and counterion cooperatively induced inversion of the stereocenter Δ/Λ and CPL in a mononuclear Eu(III) complex†

Wenhua Li, Sen Yin, Ziye Song, Pengfei Yan, Yanyan Zhou, Ting Gao * and Hongfeng Li *

The development of lanthanide complexes with stimuli-responsive dynamic chiral inversion has significant potential for applications in chiroptical switches and chiral sensing. However, the variable coordination numbers and coordination geometries of Ln(III) ions pose substantial challenges in controlling the chiral inversion of lanthanide complexes. Herein, we present the first example of solvent and counterion cooperatively induced inversion of the Eu(III) stereocenter Δ/Λ in mononuclear complexes. In $Cs[Eu(\mathbf{L}^{L})_4]$, where Cs^+ serves as the counterion, the addition of chloroform to an acetonitrile solution of the complex resulted in a reversal of Eu(III) center configuration from Δ to Λ, accompanied with an inversion of the circularly polarized luminescence (CPL) signal (g_{lum} value shifting from +0.15 to −0.13). However, when $(NMe_4)^+$ was used as the counterion, $(NMe_4)[Eu(\mathbf{L}^{L})_4]$ did not exhibit this inversion behavior under the same conditions. Notably, the addition of Cs^+ ions to a solution of $(NMe_4)[Eu(\mathbf{L}^{L})_4]$ restored the inversion feature. This understanding of the impact of Cs^+ ions and solvent on Δ/Λ inversion contributes to the development of CPL switches and sensors based on chiral lanthanide supramolecules.

Received 29th October 2024,
Accepted 28th November 2024

DOI: 10.1039/d4qi02730b

rsc.li/frontiers-inorganic

Introduction

The phenomenon of chiral inversion is widely present in biological molecules such as DNA and proteins, and the inversion is closely related to the implementation of their related functions in vital processes.[1–5] Inspired by biomacromolecules, artificial systems with chiral inversion, such as small peptides,[6,7] metal complexes,[8,9] polymers,[10,11] and supramolecules,[12,13] have been developed for their applications in fields such as asymmetric catalysis,[14,15] enantioselective recognition,[16,17] and chiral sensing.[18,19] The dynamic feature of coordination bonds and the configurational chirality (Δ or Λ) of metal centers make metal complexes an ideal platform compound for studying chiral inversion.

Recently, a few mononuclear and multinuclear complexes have achieved Δ/Λ configuration inversion under external stimuli, such as changes in solvents,[20–22] pH,[23,24] using light stimulation[25] and formation of host–guest complexes.[26,27] In the reported examples, the introduction of new coordinating atoms or the alteration of weak interactions between ligands are the main driving forces for inducing ligand rearrangements around the metal center.[28] For example, Hong and coworkers reported a chiral octahedral tris(chelate) Fe(II) complex where the modulation of hydrogen bond strength between ligands by methanol and chloroform resulted in Δ and Λ chiral inversion.[29] Miyake reported the inversion of stereochemistry from Λ to Δ in Co complexes induced by the coordination of NO_3^- ions (Scheme 1a).[30] However, these studies primarily focused on the modulation of stronger intramolecular supramolecular interactions, leaving the investigation of weaker intermolecular interactions for chirality regulation largely unexplored.

To facilitate simultaneous inversion of multiple coordination units in dynamic regulation, employing linear multidentate ligands,[31] polypodal ligands,[32] or forming multinuclear assemblies has emerged as an effective strategy.[33] The covalent linkage between coordination units enhances the mechanical coupling between ligands, thereby promoting a positive synergistic effect during ligand rearrangement. For instance, Nabeshima reported a macrocyclic copper(I) complex based on a bipodal 2,2′-bipyridine ligand, where the Δ/Λ configuration underwent inversion upon the binding of an Na^+ ion to the crown-ether-like site of the ligand (Scheme 1b).[34]

Compared to transition metal complexes, the high coordination number and variable coordination geometry of lanthanide ions necessitate the participation of a high number of ligands in the inversion process and overcome the unclear

School of Chemistry and Materials Science, Heilongjiang University, Key Laboratory of Functional Inorganic Material Chemistry, Ministry of Education, Harbin, Heilongjiang 150080, China. E-mail: lihongfeng@hlju.edu.cn, gaoting@hlju.edu.cn

†Electronic supplementary information (ESI) available. CCDC 2386501 and 2386518. For ESI and crystallographic data in CIF or other electronic format see DOI: https://doi.org/10.1039/d4qi02730b

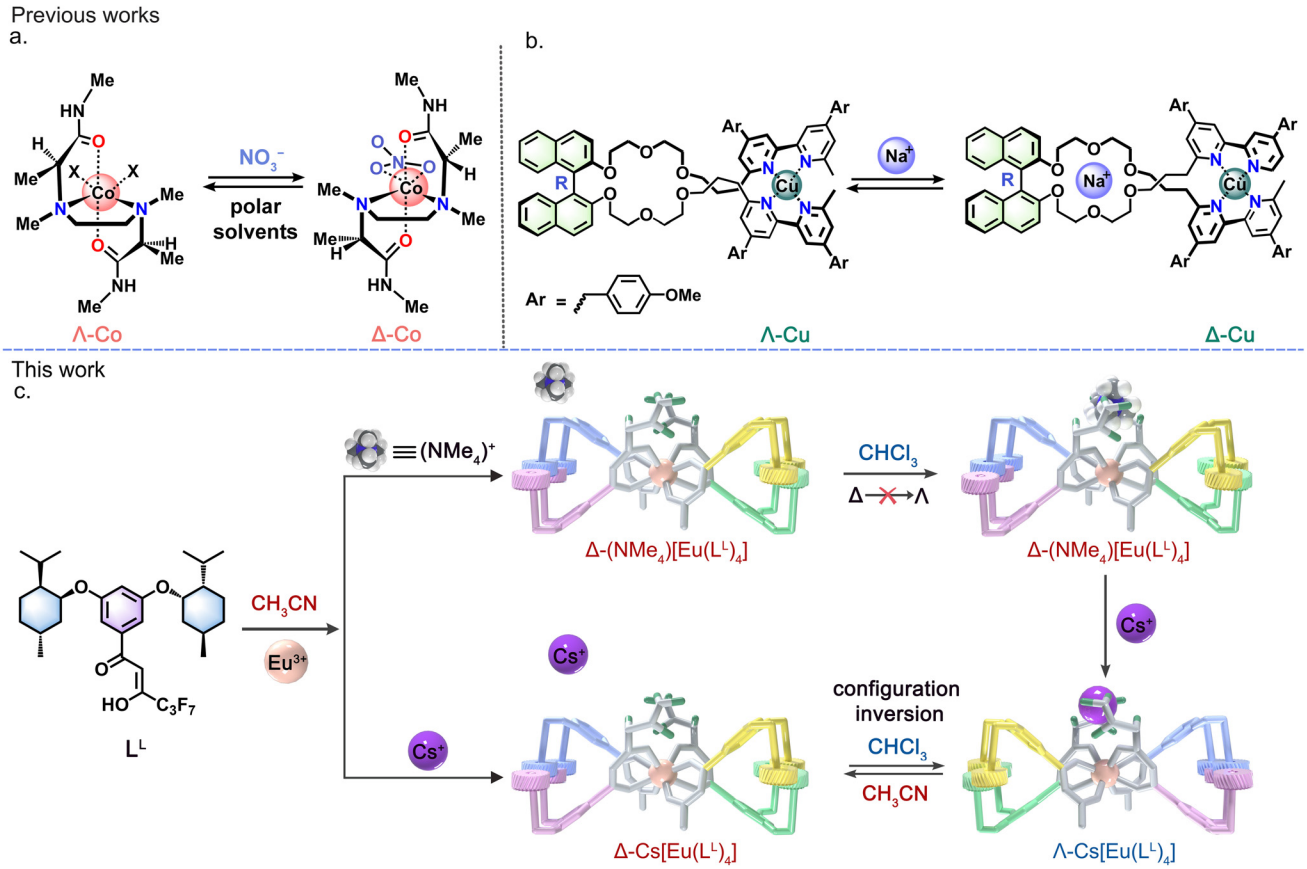

Scheme 1 Design concept of the dynamic chiral inversion of the metal center under external stimulation. (a) Schematic of NO_3^--triggered Δ/Λ inversion of Co(II) complexes. (b) The Δ/Λ configuration underwent inversion upon the binding of an Na^+ ion to the crown-ether-like site. (c) Solvent and counterion cooperatively induced inversion of Δ/Λ in $Cs[Eu(L^L)_4]$ and $(NMe_4)[Eu(L^L)_4]$.

rearrangement orientation due to the lack of coordination guidance for lanthanides, which undoubtedly increases the difficulty of regulation.[35] While several lanthanide complexes have demonstrated helicity inversion through changes in solvent polarity,[36,37] coordination to Ln(III) ions,[38,39] and changing counterions,[40–44] examples of CPL inversion remain limited.[45–48] For instance, Kawai reported a solvent-dependent CPL sign reversal, where a (+)-camphorate derivative β-diketonate Eu(III) complex exhibited a significant g_{lum} value variation from +0.66 in acetonitrile to −0.17 with increasing acetone content.[49]

Herein, we successfully report an example in which the Δ/Λ-configuration of tetrakis β-diketonate Eu(III) complexes was inverted by introducing cesium (Cs^+) as a counter cation (Scheme 1c). As the chloroform content in the acetonitrile solution of the complex increases, $Cs[Eu(\mathbf{L^L})_4]$ not only exhibits Δ → Λ configuration conversion but also causes the inversion of circularly polarized luminescence activity of Eu^{3+} ion luminescence, with the g_{lum} value flipping from +0.15 to −0.13. In contrast, the homologous $(NMe_4)[Eu(\mathbf{L^L})_4]$ with tetramethylammonium $(NMe_4)^+$ does not exhibit this inversion property. The addition of Cs^+ ions into the solution of $(NMe_4)[Eu(\mathbf{L^L})_4]$ enables realizing the Δ → Λ inversion.

Results and discussion

The design of ligands and crystal structures of $Cs[Eu(\mathbf{L^L})_4]$ and $(NMe_4)[Eu(\mathbf{L^L})_4]$

The variable coordination numbers and geometries of Ln(III) ions make the control of Δ/Λ configuration chirality in lanthanide complexes more challenging compared to that in transition metal complexes. To effectively control the chirality of Ln(III) complexes, significant steric hindrance between the ligands is required to reduce the large conformational freedom resulting from the large ionic radii and the absence of coordination directionality.[50] However, from the perspective of dynamically controlling the configurational inversion of metal complexes, such large steric hindrance is clearly detrimental to Δ/Λ reversal. Therefore, resolving the contradiction between spatial constraints and dynamic regulation for chiral configuration control necessitates the careful design of ligands. Herein, we introduced two menthol moieties at the phenyl ring of benzoyltrifluoacetone (BTFA), forming a symmetric "tripodal" structure (Scheme 1c). The menthol group possesses molecular chirality, moderate rigidity–flexibility, and a large volume. When forming the $Eu(\mathbf{L^L})_4$ structure, the convergence of the eight menthol units around the Eu^{3+} ion

within the limited space is expected to control the unidirectional arrangement of the ligands through weak interactions between the menthol groups and/or benzene rings. On the other hand, the moderate flexibility of menthol provides a structural basis for conformational adjustment to accommodate Δ/Λ configuration inversion under external stimuli. Additionally, the negative charge of $[Eu(\mathbf{L}^{\mathbf{L}})_4]^-$ enables the possibility of utilizing a cation to regulate structural transformations. To enhance the ion-pair interaction, we employed multi-fluoroalkyl groups as the terminal substituents of BTFA, which can engage in strong multiple hydrogen bonding or ion-dipole supramolecular interactions with $(NMe_4)^+$ and Cs^+ ions.

The synthesis and characterization of enantiomerically pure $\mathbf{L}^{\mathbf{L}}$ and $\mathbf{L}^{\mathbf{D}}$, as well as their corresponding complexes $Cs[Eu(\mathbf{L}^{\mathbf{L/D}})_4]$ and $(NMe_4)[Eu(\mathbf{L}^{\mathbf{L/D}})_4]$, are listed in Scheme S1 and Fig. S1–S24.† $Cs[Eu(\mathbf{L}^{\mathbf{L/D}})_4]$ and $(NMe_4)[Eu(\mathbf{L}^{\mathbf{L/D}})_4]$ were prepared by reacting ligand $\mathbf{L}^{\mathbf{L/D}}$ and Eu^{3+} in a 4 : 1 ratio in acetonitrile, using cesium hydroxide (CsOH, 50% w/w in water) and tetramethylammonium hydroxide (25% w/w in water) as bases, respectively. The formation of the complexes was confirmed by single-crystal X-ray diffraction analysis. Colorless crystals of $Cs[Eu(\mathbf{L}^{\mathbf{L}})_4]$ and $(NMe_4)[Eu(\mathbf{L}^{\mathbf{L}})_4]$, suitable for single-crystal X-ray diffraction, were obtained by slow evaporation of their acetonitrile/acetone/methanol-containing solutions. Crystallographic analysis revealed that $Cs[Eu(\mathbf{L}^{\mathbf{L}})_4]$ crystallizes in the Sohncke space group $C2$, while $(NMe_4)[Eu(\mathbf{L}^{\mathbf{L}})_4]$ crystallizes in the Sohncke space group $P2_12_12$. Notably, $Cs[Eu(\mathbf{L}^{\mathbf{L}})_4]$ exhibits a pseudo-racemate with Δ- and Λ-isomers in a 1 : 1 ratio within the crystal structure (Fig. 1a). In each Δ- or Λ-isomer, four ligands coordinate to the Eu^{3+} ion in a head-to-tail alternating arrangement (C_3F_7 as heads and menthol tails), with four menthol groups on two ligands adopting interdigitated arrangement (Scheme 1c, menthol group denoted with a cartoon gear). This arrangement leads to multiple hydrophobic interactions between the adjacent menthol groups, with H···H distances ranging from 1.8 to 3.9 Å. Notably, the methyl and isopropyl groups on one menthol moiety exhibit C–H···π interactions with the benzene ring of a neighboring ligand, with distances ranging from 2.5 to 3.8 Å. The Cs^+ counterion is located within the cavity formed by the perfluoroalkyl chains and menthol groups, engaging in ion-dipole interactions with fluorine atoms (Cs···F distance, 3.1 to 3.4 Å).

In contrast to $Cs[Eu(\mathbf{L}^{\mathbf{L}})_4]$, $(NMe_4)[Eu(\mathbf{L}^{\mathbf{L}})_4]$ adopts only a Λ configuration, lacking the pseudo-racemate Δ- and the Λ-isomer pair. Furthermore, the ligand arrangement differs

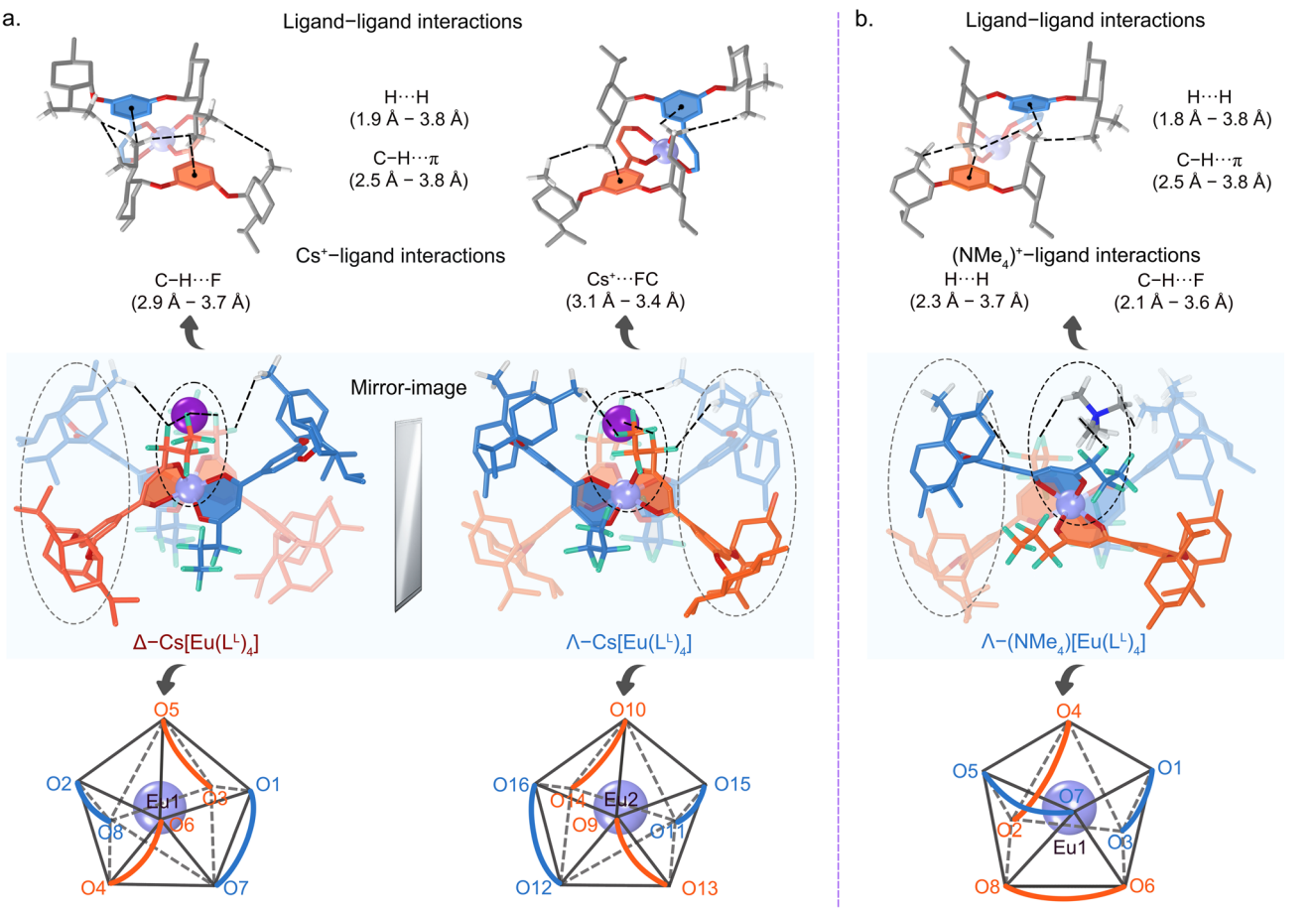

Fig. 1 X-ray crystallographic structures and coordination geometries of (a) $Cs[Eu(\mathbf{L}^{\mathbf{L}})_4]$ and (b) $(NMe_4)[Eu(\mathbf{L}^{\mathbf{L}})_4]$ (color codes: Eu, blue-purple sphere; O, red; F, green; Cs, purple sphere). Some atoms are omitted for clarity.

between the two complexes. In Cs[Eu($\mathbf{L}^{\mathbf{L}}$)$_4$], eight oxygen atoms surrounding the Eu^{3+} ion form a triangular dodecahedron coordination geometry, with each ligand located at the edge of the polyhedron. In (NMe_4)[Eu($\mathbf{L}^{\mathbf{L}}$)$_4$], the eight oxygen atoms form a square antiprism (SAP) coordination geometry. Notably, two bidentate diketonate units (O5, O7 and O6, O8) are located on the square planes of the SAP. The $(NMe_4)^+$ counterion resides within the cavity formed by the polyfluoroalkyl chains and menthol groups. The H···H and C–H···F distances between the $(NMe_4)^+$ and the ligands are in the range of 2.3 to 3.7 Å and 2.1 to 3.6 Å, respectively.

Solvent-induced inversion of Eu(III) stereocenter Δ/Λ and CPL

The presence of diastereoisomeric Δ-Eu($\mathbf{L}^{\mathbf{L}}$)$_4$ and Λ-Eu($\mathbf{L}^{\mathbf{L}}$)$_4$ in the crystalline state suggests that the menthol groups in the ligand do not provide sufficient steric hindrance to favor the formation of a single diastereoisomer. This observation implies that the complexes possess the potential for dynamic interconversion between Λ and Δ configurations in the solution upon exposure to external stimuli. To investigate this possibility, the solution structures of the two complexes were initially characterized in acetonitrile. High-resolution mass spectrometry (HR-MS) confirmed the formation of tetrakis β-diketonate complexes Cs[Eu($\mathbf{L}^{\mathbf{L/D}}$)$_4$] and (NMe_4)[Eu($\mathbf{L}^{\mathbf{L/D}}$)$_4$], where the isotopic distribution of the molecular ion peaks corresponding to the anionic species [Eu($\mathbf{L}^{\mathbf{L}}$)$_4$]$^-$ closely matches the simulated distribution (Fig. 2a). Notably, the ^{1}H NMR spectra of the complex Cs[Eu($\mathbf{L}^{\mathbf{L}}$)$_4$] exhibited a single set of signals (Fig. 2b), rather than the anticipated two sets of peaks associated with the Δ and Λ diastereoisomers observed in the crystalline state. This suggests that the complex Cs[Eu($\mathbf{L}^{\mathbf{L}}$)$_4$] either exists as a single Λ- or Δ-configurational isomer in the solution or undergo rapid interconversion between the two isomers. In the case of (NMe_4)[Eu($\mathbf{L}^{\mathbf{L}}$)$_4$], the protons of the counterion $(NMe_4)^+$ appeared at 3.09 ppm, which aligns with the chemical shift of the free $(NMe_4)^+$ in acetonitrile at 3.07 ppm (Fig. S25†), indicating complete dissociation of $(NMe_4)^+$ from [Eu($\mathbf{L}^{\mathbf{L}}$)$_4$]$^-$. Based on this observation, we speculate that the absence of ion-pair interaction likely facilitates the Λ ↔ Δ configurational conversion.

Circular dichroism (CD) spectroscopy is one of the most useful techniques for analyzing the configuration of metal complexes. As depicted in Fig. 2c, the CD spectrum of (NMe_4)[Eu($\mathbf{L}^{\mathbf{L}}$)$_4$] exhibits a distinct Cotton effect within the ligand absorption band, ranging from 250 to 380 nm. The negative exciton couplet observed in this spectrum suggests an Δ con-

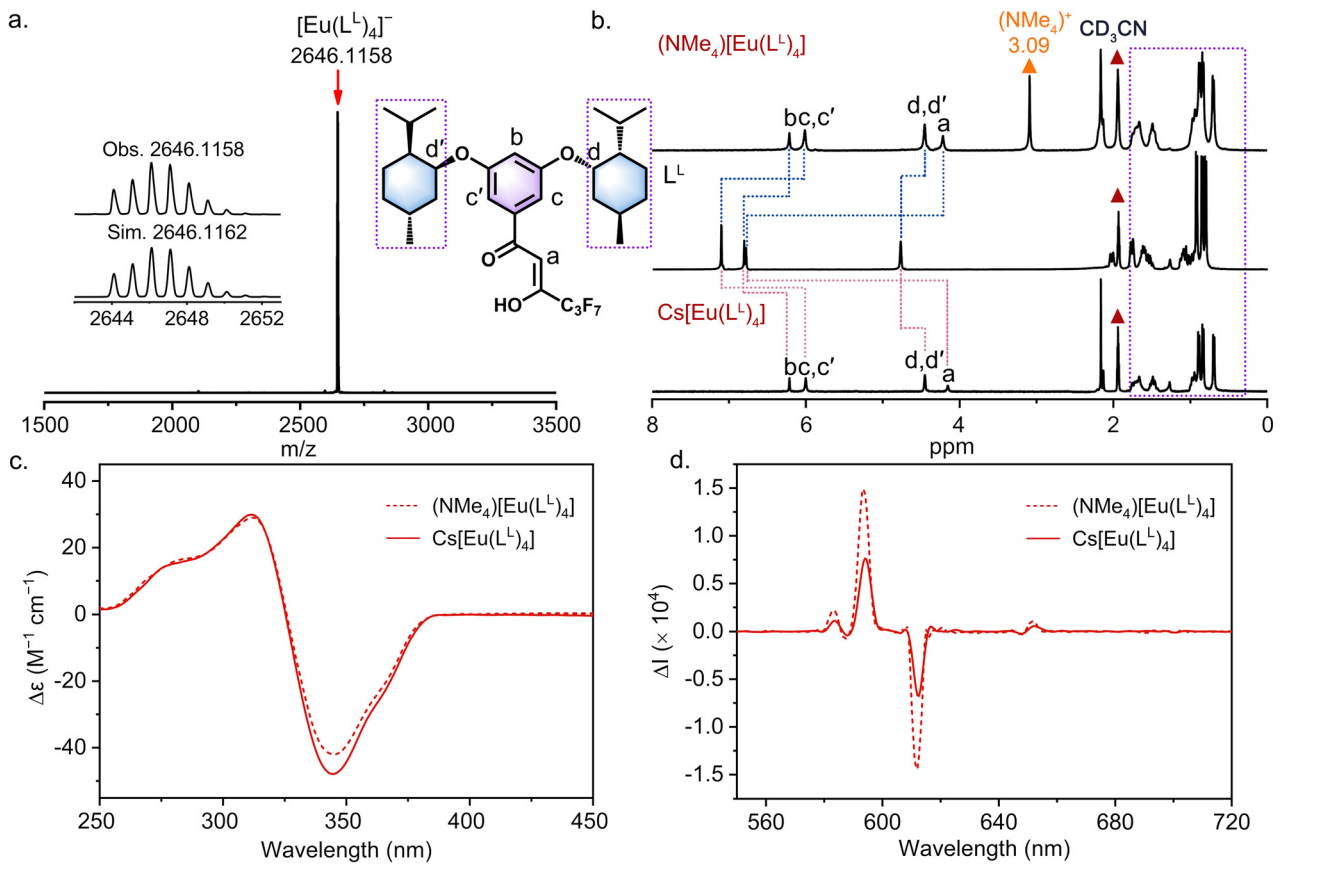

Fig. 2 (a) ESI-MS spectrum of (NMe_4)[Eu($\mathbf{L}^{\mathbf{L}}$)$_4$] in CH_3CN. (b) ^{1}H NMR spectra of free ligand $\mathbf{L}^{\mathbf{L}}$, (NMe_4)[Eu($\mathbf{L}^{\mathbf{L}}$)$_4$] and Cs[Eu($\mathbf{L}^{\mathbf{L}}$)$_4$] in CD_3CN (400 MHz, 298 K). (c) CD spectra of (NMe_4)[Eu($\mathbf{L}^{\mathbf{L}}$)$_4$] (red dashed line) and Cs[Eu($\mathbf{L}^{\mathbf{L}}$)$_4$] in CH_3CN (c = 1.0 × 10^{-4} M). (d) CPL spectra of (NMe_4)[Eu($\mathbf{L}^{\mathbf{L}}$)$_4$] (red dashed line) and Cs[Eu($\mathbf{L}^{\mathbf{L}}$)$_4$] in CH_3CN (c = 1.0 × 10^{-5} M).

figuration at the Eu^{3+} ion center.[51] Consistent with this finding, the circularly polarized luminescence (CPL) spectra of $(NMe_4)[Eu(\mathbf{L}^{\mathbf{L}})_4]$ exhibit a positive sign at the magnetic dipole $^5D_0 \rightarrow {}^7F_1$ transition (595 nm) and a negative sign at the electron dipole $^5D_0 \rightarrow {}^7F_2$ transition (612 nm), further indicating a Δ configuration at the Eu^{3+} ion center.[52–54] Similarly, the CD and CPL spectra of $Cs[Eu(\mathbf{L}^{\mathbf{L}})_4]$ in CH_3CN display spectral patterns identical to those observed in $(NMe_4)[Eu(\mathbf{L}^{\mathbf{L}})_4]$, confirming the Δ configuration of the metal center (Fig. 2d). These findings indicate a Λ → Δ configurational conversion upon dissolution of the crystalline complexes in CH_3CN.

Based on the hypothesis that the ion pair dissociation in acetonitrile drives the configuration conversion, we propose that reducing ion pair dissociation by introducing a weakly polar solvent will hinder this conversion, potentially even reversing the configuration from Δ to Λ. To investigate this possibility, we selected chloroform ($CHCl_3$) as a weakly polar solvent to study the potential inverse process. In the ^1H NMR spectrum, the significant downfield shift of $(NMe_4)^+$ from 3.09 ppm to 16.53 ppm in $CDCl_3$ strongly suggests the formation of an ion pair (Fig. 3b). This substantial shift is attributed to the paramagnetic effect of the Eu^{3+} ion. Additionally, the identical diffusion coefficients of $(NMe_4)^+$ and $[Eu(\mathbf{L}^{\mathbf{L}})_4]^-$ in ^1H DOSY further support the formation of an ion pair (Fig. S14†). However, the CD spectrum (Fig. 3c) of $(NMe_4)[Eu(\mathbf{L}^{\mathbf{L}})_4]$ in $CHCl_3$ exhibits the same exciton coupling pattern as that observed in CH_3CN, indicating that the ion pair formation does not lead to a reversal of the configuration. A slight variation is observed in the luminescence dissymmetry factor (g_{lum}, $^5D_0 \rightarrow {}^7F_1$, 595 nm), which increases from +0.142 to +0.197.

In contrast, $Cs[Eu(\mathbf{L}^{\mathbf{L/D}})_4]$ exhibits a configurational inversion in $CHCl_3$, as evidenced by the reversed CD and CPL spectra. As shown in Fig. 3e, the CD spectrum displays a posi-

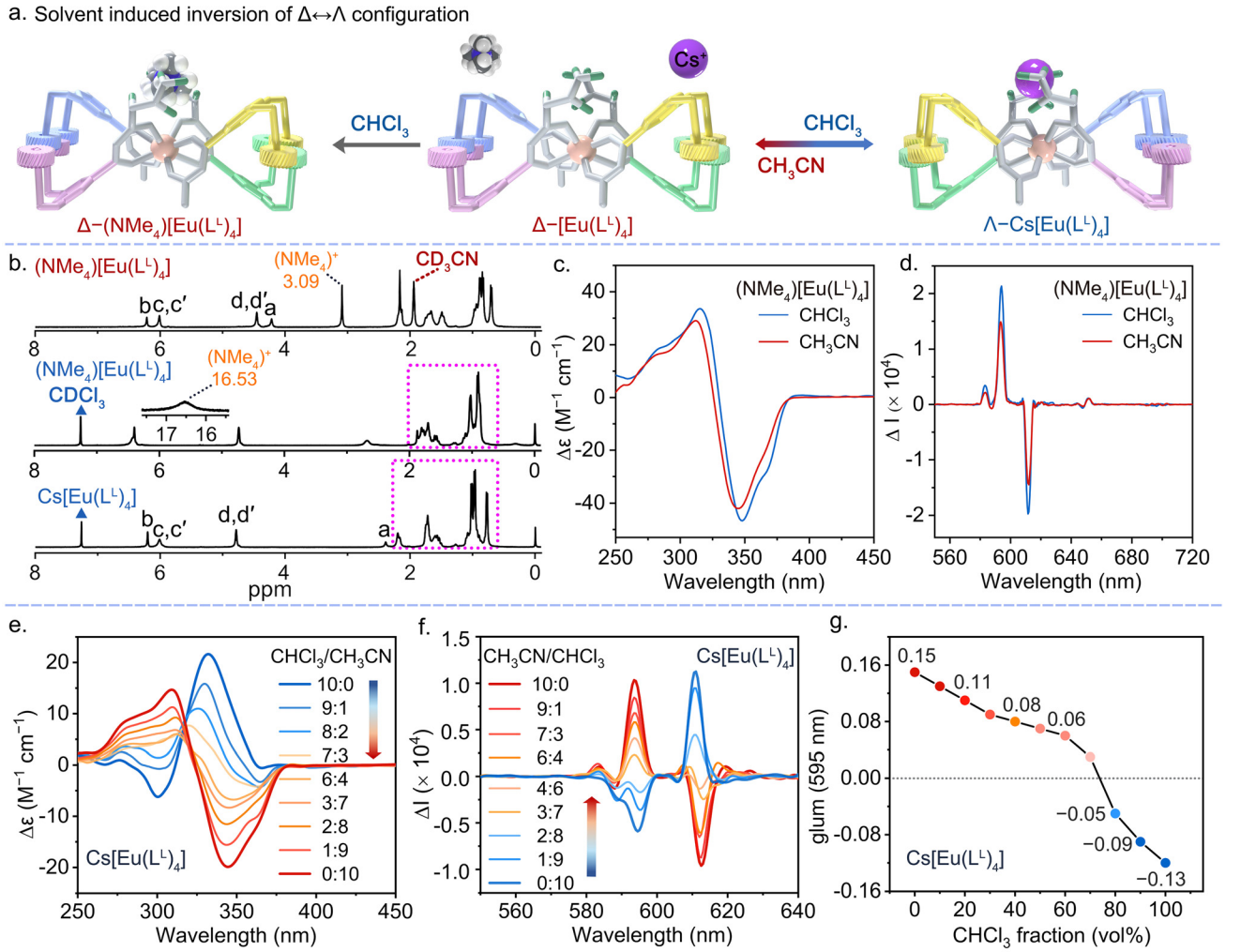

Fig. 3 Solvent-induced inversion of Eu(III) stereocenter Δ/Λ and CPL. (a) Solvent induced Δ ⇌ Λ inversion of $Cs[Eu(\mathbf{L}^{\mathbf{L}})_4]$. (b) ^1H NMR spectra of $(NMe_4)[Eu(\mathbf{L}^{\mathbf{L}})_4]$ in $CDCl_3$ and CD_3CN and ^1H NMR spectra of $Cs[Eu(\mathbf{LL})_4]$ in $CDCl_3$ (400 MHz, 298 K). (c) CD spectra of $(NMe_4)[Eu(\mathbf{L}^{\mathbf{L}})_4]$ in CH_3CN and $CHCl_3$ (c = 1.0 × 10^{-4} M). (d) CPL spectra of $(NMe_4)[Eu(\mathbf{L}^{\mathbf{L}})_4]$ in CH_3CN and $CHCl_3$ (c = 1.0 × 10^{-5} M). (e) CD spectral changes in $Cs[Eu(\mathbf{L}^{\mathbf{L}})_4]$ with increasing $CHCl_3$ content in CH_3CN (c = 2.5 × 10^{-5} M). (f) CPL spectral changes of $Cs[Eu(\mathbf{L}^{\mathbf{L}})_4]$ with increasing $CHCl_3$ content in CH_3CN (c = 1.0 × 10^{-5} M). (g) The g_{lum} value changes of $Cs[Eu(\mathbf{LL})_4]$ with increasing $CHCl_3$ content in CH_3CN.

tive exciton couplet, while the CPL spectrum (Fig. 3f) exhibits a negative signal at 595 nm and a positive signal at 612 nm, both suggesting a Λ configuration of the complex in $CHCl_3$. This finding indicates that the configuration conversion can be induced in the solution by varying the solvent composition. As expected, both CD and CPL spectra reveal an inversion process upon increasing the chloroform content in CH_3CN. The CD spectrum demonstrates that the molar extinction coefficient $\Delta\varepsilon = -20\ M^{-1}\ cm^{-1}$ undergoes a signal reversal at a $CH_3CN/CHCl_3$ volume ratio of 3/7, eventually reaching a maximum positive value in chloroform ($\Delta\varepsilon = 23\ M^{-1}\ cm^{-1}$). Similarly, the CPL spectrum also exhibits a signal inversion, accompanied by a g_{lum} value inversion from +0.15 to −0.13 (Fig. 3g). This Δg_{lum} value of 0.28 is considerably larger and more practically useful compared to the conventional $\Delta g < 10^{-2}$ CPL reversal magnitude change observed in fluorescent dyes.[55] Additionally, subtle differences in the fine structure of the emission spectra (Fig. S44†) indicate variations in the Eu^{3+} ion coordination environment in acetonitrile and chloroform. Different solvents also result in distinct luminescence quantum yields (QYs) for $Cs[Eu(\mathbf{L^L})_4]$, with values of 36% ($CHCl_3$) and 45% (CH_3CN). The high QYs benefit from the good energy level match between the triplet state (T_1, 20 400 cm^{-1}) of the ligand (estimated from the 0 → 0 transition of $Cs[Gd(\mathbf{L^L})_4]$) (Fig. S47†) and the $^5D_0$ energy of the Eu^{3+} ion.

This solvent-dependent inversion process was also monitored by ^1H NMR spectroscopy (Fig. S54†). As the chloroform ($CDCl_3$) content increased, the peaks of all the protons exhibited broadening, particularly those from the methyl group (H_a) and the menthol moiety protons ($H_{d,d'}$). However, no two sets of signals associated with the Δ and Λ diastereoisomers were observed. To avoid the influence of the peak broadening on spectral resolution caused by the paramagnetism of the Eu^{3+} ion, the isomorphic $Cs[Lu(\mathbf{L^L})_4]$ was used as a substitute for the ^1H NMR experiment (Fig. S55†). However, the ^1H NMR spectra still displayed a single set of signals, indicating that a rapid Δ ↔ Λ interconversion between the two isomers occurred within the timescale of the ^1H NMR experiment. Although the content ratio of Δ- and Λ-$Cs[Lu(\mathbf{L^L})_4]$ diastereoisomers cannot be accurately determined, the chiroptical variations unequivocally verify the existence of configurational inversion at the Eu^{3+} ion center and demonstrate the role of the Cs^+ ion in dynamic chirality reversal regulation.

Mechanism of the Eu^{3+} stereocenter Δ/Λ inversion

The aforementioned ^1H NMR, ESI-TOF-MS, and chiroptical experiments have established a correlation between configuration reversal and enhanced ion pair interactions. In polar CH_3CN, the strong solvation effect on the anion and cation leads to complete dissociation of Cs^+ and $[Eu(\mathbf{L^L})_4]^-$. This indicates that the complex exhibits a stereochemical preference for the Δ configuration in the absence of a counterion. To validate this hypothesis, DFT calculations were performed to optimize the structures of Δ-$[Eu(\mathbf{L^L})_4]^-$ and Λ-$[Eu(\mathbf{L^L})_4]^-$ in the absence

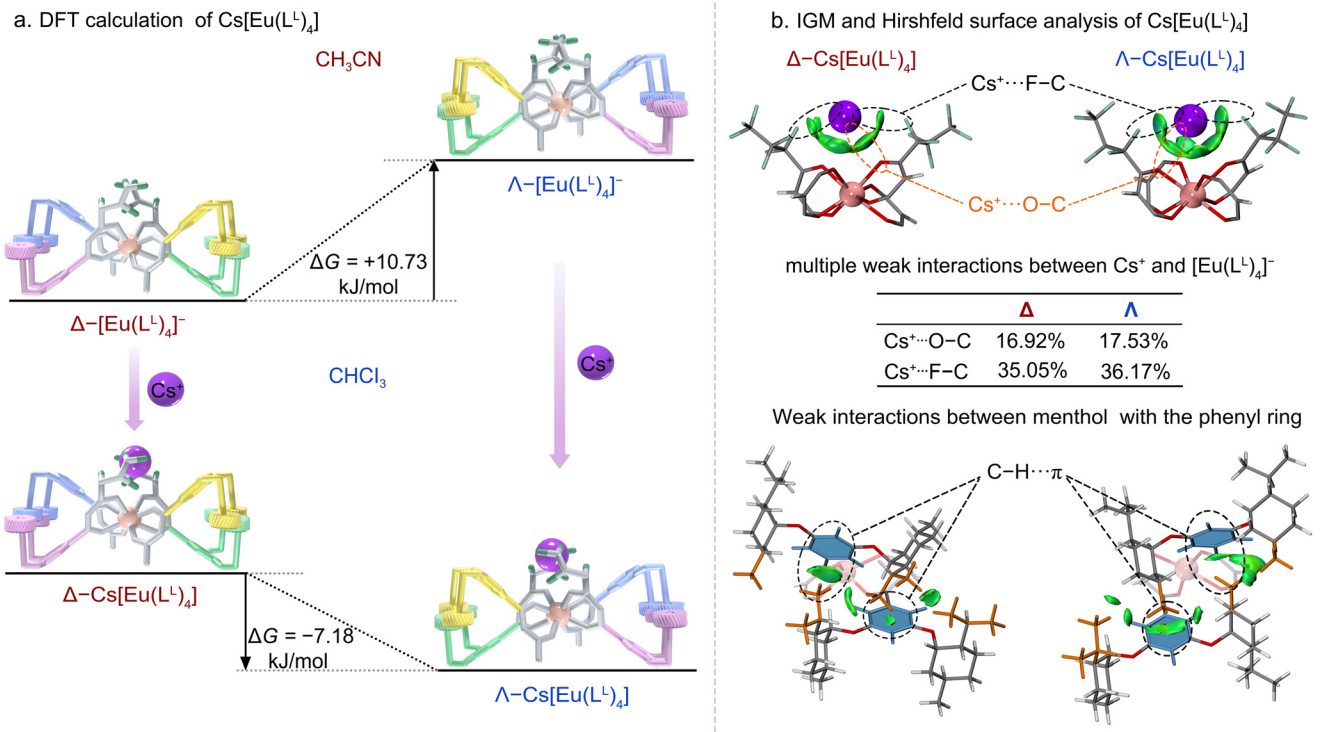

Fig. 4 DFT calculation (energies are given in kJ mol^{-1}), IGM and Hirshfeld surface analysis of Δ/Λ-$Cs[Eu(LL)_4]$. (a) Energy diagrams of the Δ/Λ-$Cs[Eu(LL)_4]$ in the absence and presence of the counterion Cs^+. (b) IGM and Hirshfeld surface analysis of the weak interactions of Δ/Λ-$Cs[Eu(LL)_4]$ (δg_{inter} = 0.008). The percentage represents the contribution of C−F···Cs and C−O···Cs contacts to the total Hirshfeld surface area between Cs^+ and the complexes.

of counterions, mimicking the situation of the complexes in CH_3CN. The initial structural coordinates were obtained directly from the crystal structure. Precise energy calculations revealed that the free Δ-$[Eu(\mathbf{L}^{L})_4]^-$ exhibits lower system energy compared to the Λ-$[Eu(\mathbf{L}^{L})_4]^-$ isomer (ΔG = +10.73 kJ mol^{-1}). This suggests that Δ-$[Eu(\mathbf{L}^{L})_4]^-$ is the thermodynamically stable product in the absence of counterions, consistent with the predictions of a Δ configuration or an excess of the Δ configuration inferred from CD and CPL spectra in CH_3CN. The optimized structures and calculated system energies are depicted in Fig. 4a and S56.†

To verify the inversion arising from the interaction between Cs^+ and $[Eu(\mathbf{L}^{L})_4]^-$, geometry optimizations and energy calculations were performed on the ion pairs, Δ-$Cs[Eu(\mathbf{L}^{L})_4]$ and Λ-$Cs[Eu(\mathbf{L}^{L})_4]$ (Fig. 4a and S57†). As expected, with Cs^+ as the counterion, Λ-$Cs[Eu(\mathbf{L}^{L})_4]$ exhibits a lower system energy than Δ-$Cs[Eu(\mathbf{L}^{L})_4]$ (ΔG = −7.18 kJ mol^{-1}). This result aligns with the deduction of a $\Delta \rightarrow \Lambda$ conversion due to the formation of ion pairs in $CHCl_3$. While the calculated ΔG was consistent with the experimental inversion results, DFT calculations have limitations, such as a computational accuracy of only 8.5–13.0 kJ mol^{-1}.[56] Therefore, DFT calculations can only provide a reference for this inversion process from the thermodynamic point of view. However, from the observed trends of energy, uphill and downhill in the complex, before and after Cs^+ ion binding, we believe that the DFT results still support

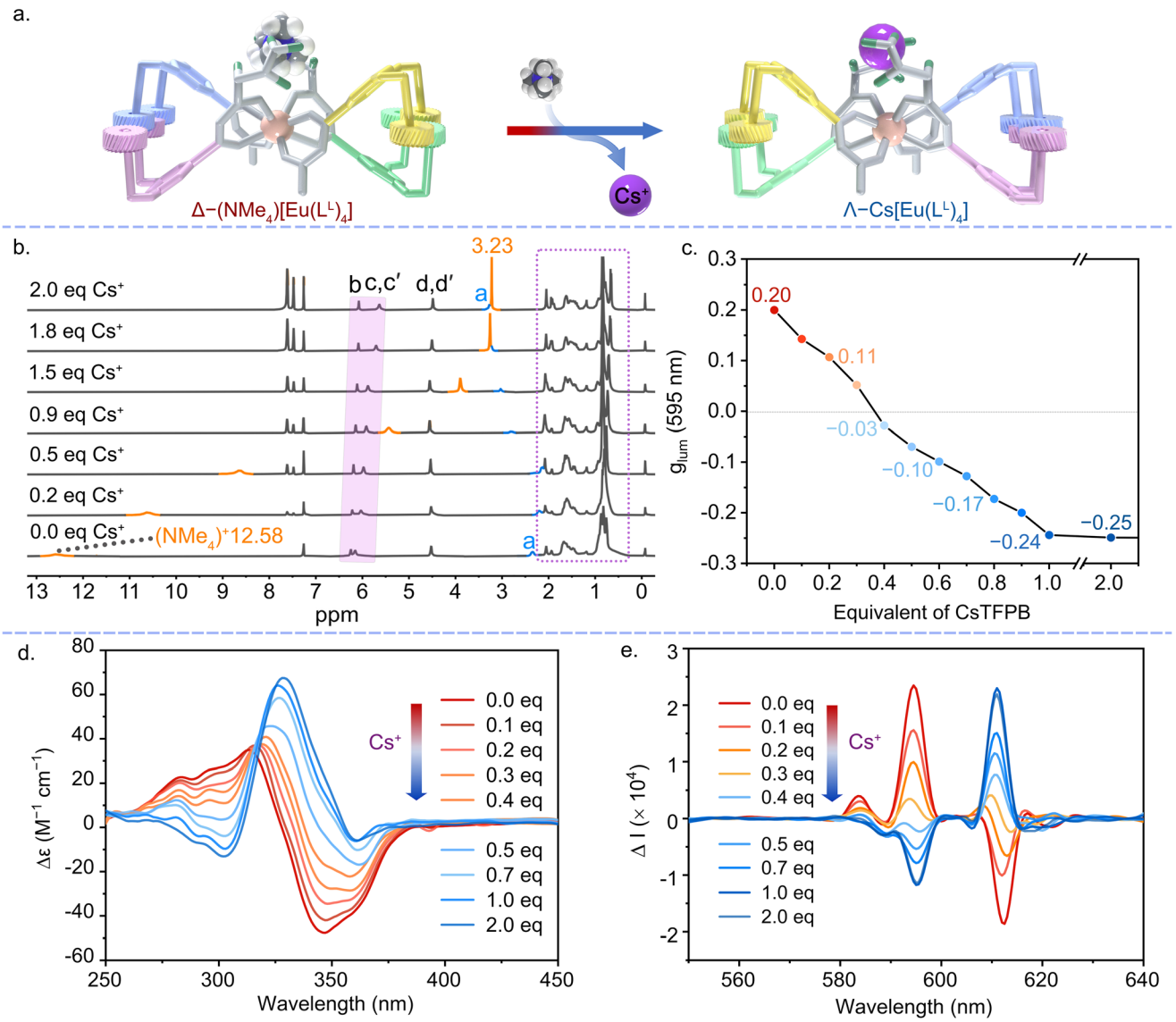

Fig. 5 Counterion exchange induced inversion of $\Delta \rightarrow \Lambda$ and CPL. (a) Configuration inversion of Δ-$(NMe_4)[Eu(\mathbf{L}^{L})_4] \rightarrow \Lambda$-$Cs[Eu(\mathbf{L}^{L})_4]$ triggered by counterion exchanging. (b) Changes in ^{1}H NMR spectral upon adding various equivalents of Cs^+ to the solution of $(NMe_4)[Eu(\mathbf{L}^{L})_4]$ (400 MHz, 298 K, $CD_3CN/CDCl_3$ = 1 : 9). (c) Changes in the g_{lum} value upon adding various equivalents of CsTFPB to the solution of $(NMe_4)[Eu(\mathbf{L}^{L})_4]$ in $CH_3CN/CHCl_3$ (1 : 9, v/v). (d) Changes in CD spectral upon adding various equivalents of Cs^+ (c = 7.0 × 10^{-3} M) to the solution of $(NMe_4)[Eu(\mathbf{L}^{L})_4]$ (c = 1.0 × 10^{-4} M) in $CH_3CN/CHCl_3$ (1 : 9, v/v). (e) Changes in CPL spectral upon adding various equivalents of Cs^+ (c = 1.5 × 10^{-3} M) to the solution of $(NMe_4)[Eu(\mathbf{L}^{L})_4]$ (c = 1.0 × 10^{-5} M) in $CH_3CN/CHCl_3$ (1 : 9, v/v).

the assertion that ion pairing can alter the thermodynamic equilibrium between diastereomers.

To further elucidate the influence of counterions (Cs^+) on the thermodynamic stability of Δ- and Λ-isomers, non-covalent interactions between Cs^+ and $[Eu(\mathbf{L}^{\mathbf{L}})_4]^-$ were investigated using independent gradient model (IGM) analysis and Hirshfeld surface analysis.[57–59] The IGM analysis revealed green regions between Cs^+ and $[Eu(\mathbf{L}^{\mathbf{L}})_4]^-$, indicating the presence of various weak intermolecular interactions (Fig. 4b). To quantify these supramolecular interactions, Hirshfeld surface analysis was conducted. This analysis highlighted strong contacts between Cs^+ and $[Eu(\mathbf{L}^{\mathbf{L}})_4]^-$, predominantly driven by C–F···Cs and C–O···Cs interactions. The results showed that compared to Δ-Cs$[Eu(\mathbf{L}^{\mathbf{L}})_4]$, the contacts between Cs^+ and $[Eu(\mathbf{L}^{\mathbf{L}})_4]^-$ are closer in Λ-Cs$[Eu(\mathbf{L}^{\mathbf{L}})_4]$, with a larger contribution from C–F···Cs interactions (35.05% for Δ-Cs$[Eu(\mathbf{L}^{\mathbf{L}})_4]$ and 36.17% for Λ-Cs$[Eu(\mathbf{L}^{\mathbf{L}})_4]$). Additionally, various weak interactions were observed between the menthol groups in the neighboring ligands and the menthol/benzene ring. IGM analysis indicated that the contact areas between ligands are greater in Λ-Cs$[Eu(\mathbf{L}^{\mathbf{L}})_4]$ compared to those in Δ-Cs$[Eu(\mathbf{L}^{\mathbf{L}})_4]$ (C–H···π) (Fig. S59†). These results demonstrate that the energy difference between the two stereoisomeric pairs, estimated from DFT calculations, likely arises from variations in these weak interaction strengths. Overall, the DFT calculations and weak interaction analyses provide strong evidence for the solvent- and counterion-dependent inversion process.

Counterion exchange induced inversion of Δ → Λ and CPL

The above CD and CPL titration experiments show that the chiral inversion of the complexes is not only dependent on the solvent but also on the selection of counterions, Cs^+ and $(NMe_4)^+$. Therefore, we speculate that the addition of Cs^+ ions to the solution of $(NMe_4)[Eu(\mathbf{L}^{\mathbf{L}})_4]$ probably results in the replacement of $(NMe_4)^+$, and induces the configurational inversion from Δ to Λ. The ^{1}H NMR titration experiment demonstrates the occurrence of ion exchange. As depicted in Fig. 5b, upon adding various equivalents of the Cs^+ ion to the CD_3CN/$CDCl_3$ (1 : 9, v/v) solution of $(NMe_4)[Eu(\mathbf{L}^{\mathbf{L}})_4]$, all proton resonances underwent shifts, with the methyl group of $(NMe_4)^+$ exhibiting the most significant change. When 2.0 equivalents of Cs^+ were introduced, the methyl signal of $(NMe_4)^+$ shifted from the initial 12.58 ppm to 3.23 ppm, very close to the chemical shift of the free $(NMe_4)^+$ at 3.20 ppm (Fig. S65†), indicating the complete replacement of $(NMe_4)^+$ by Cs^+. The fitting results obtained using BindFit software demonstrated that the binding of Cs^+ with $[Eu(\mathbf{L}^{\mathbf{L}})_4]^-$ follows a 1 : 1 binding model, with a calculated relative binding constant $K = K_{Cs}/K_{(NMe_4)}$ = 303 M^{-1} (Fig. S63†).

CD and CPL spectra provided further evidence for the role of counterion exchange in regulating the Δ → Λ configuration inversion. As depicted in Fig. 5d, upon the addition of varying amounts of the Cs^+ salt, the CD spectrum gradually transitions from negative exciton coupling to a positive form, reaching a maximum value of 75 M^{-1} cm^{-1} at approximately 2.0 eq. of Cs^+ (Fig. S67†). A similar trend was observed in the CPL spectrum (Fig. 5e). Initially, $(NMe_4)[Eu(\mathbf{L}^{\mathbf{L}})_4]$ exhibits a positive CPL signal at the $^5D_0 \rightarrow {}^7F_1$ transition, with a g_{lum} value of +0.20. However, with the introduction of Cs^+ salt, the CPL signal intensity gradually diminishes, and at around 0.4 eq. of Cs^+, the CPL sign begins to invert, eventually reaching a maximum negative value of −0.25 at approximately 2.0 eq. of Cs^+ (Fig. S68 and S69†). The g_{lum} value varies with the changing Cs^+ equivalents, as shown in Fig. 5c. Additionally, the replacement of $(NMe_4)^+$ by Cs^+ is also evident in the alterations of the emission spectral pattern for the $^5D_0 \rightarrow {}^7F_2$ transition (Fig. S70†).

Conclusions

In summary, we present a case demonstrating that the chiral inversion of a mononuclear Eu(III) complex is dependent on the cooperative effect of the solvent and the counterion. The enhanced ion pair interaction between the Cs^+ ion and the anionic $[Eu(\mathbf{L}^{\mathbf{L}})_4]^-$, driven by a decrease in solvent polarity, was shown to be the driving force for this configurational conversion. However, the absence of inversion for $(NMe_4)[Eu(\mathbf{L}^{\mathbf{L}})_4]$ indicates that the inversion is not solely determined by ion-pair interaction but also by the stereochemical preference of the final complex. These findings offer a novel perspective on studying dynamic chirality reversal in lanthanide complexes, highlighting their unique potential as CPL switches due to substantial variations in the CPL signal (Δg_{lum} = 0.28 in this work).

Author contributions

H. F. L. conceived and supervised the project. W. H. L. performed the experiments and analyzed the data. S. Y. and Z. Y. S. collected diffraction data and solved and refined the X-ray crystal structures. H. F. L., T. G., Y. Y. Z. and P. F. Y. reviewed and edited the paper. All authors contributed to the final draft of the paper.

Data availability

The data that supports the findings of this study are available in the ESI† of this article.

Conflicts of interest

There are no conflicts to declare.

Acknowledgements

This work was financially supported by the National Natural Science Foundation of China (no. 52273263, 52203219 and 52073080), Heilongjiang Provincial Natural Science

Foundation Joint Guidance Projects (no. LH2023B022), Scientific Research Project of Basic Scientific Research Operating Expenses of Colleges and Universities in Heilongjiang Province (2021-KYYWF-0029 and 2021-KYYWF-0041). Heilongjiang Province key research and development plan (2022ZX07D04).

References

1 B. Dumat, A. F. Larsen and L. M. Wilhelmsson, Studying Z-DNA and B- to Z-DNA transitions using a cytosine analogue FRET-pair, *Nucleic Acids Res.*, 2016, **44**, e101.
2 F. M. Pohl, Dynamics of the B-to-Z transition in supercoiled DNA, *Proc. Natl. Acad. Sci. U. S. A.*, 1986, **83**, 4983–4987.
3 A. Rich and S. Zhang, Z-DNA: the long road to biological function, *Nat. Rev. Genet.*, 2003, **4**, 566–572.
4 S. J. Klawa, M. Lee, K. D. Riker, T. Jian, Q. Wang, Y. Gao, M. L. Daly, S. Bhonge, W. S. Childers, T. O. Omosun, A. K. Mehta, D. G. Lynn and R. Freeman, Uncovering supramolecular chirality codes for the design of tunable biomaterials, *Nat. Commun.*, 2024, **15**, 788.
5 C. Mao, W. Sun, Z. Shen and N. C. Seeman, A nanomechanical device based on the B-Z transition of DNA, *Nature*, 1999, **397**, 144–146.
6 N. Ousaka, Y. Takeyama, H. Iida and E. Yashima, Chiral information harvesting in dendritic metallopeptides, *Nat. Chem.*, 2011, **3**, 856–861.
7 N. Ousaka, Y. Takeyama and E. Yashima, Anion-driven reversible switching of metal-centered stereoisomers in metallopeptides, *Chem. – Eur. J.*, 2013, **19**, 4680–4685.
8 W. Xue, L. Pesce, A. Bellamkonda, T. K. Ronson, K. Wu, D. Zhang, N. Vanthuyne, T. Brotin, A. Martinez, G. M. Pavan and J. R. Nitschke, Subtle stereochemical effects influence binding and purification abilities of an $Fe^{II}{}_4L_4$ cage, *J. Am. Chem. Soc.*, 2023, **145**, 5570–5577.
9 S. A. Ikbal, P. Zhao, M. Ehara and S. Akine, Acceleration and deceleration of chirality inversion speeds in a dynamic helical metallocryptand by alkali metal ion binding, *Sci. Adv.*, 2023, **9**, eadj5536.
10 R. Ishidate, A. J. Markvoort, K. Maeda and E. Yashima, Unexpectedly strong chiral amplification of chiral/achiral and chiral/chiral copolymers of biphenylylacetylenes and further enhancement/inversion and memory of the macromolecular helicity, *J. Am. Chem. Soc.*, 2019, **141**, 7605–7614.
11 K. Shimomura, T. Ikai, S. Kanoh, E. Yashima and K. Maeda, Switchable enantioseparation based on macromolecular memory of a helical polyacetylene in the solid state, *Nat. Chem.*, 2014, **6**, 429–434.
12 S. G. Kang, K. Y. Kim, Y. Cho, D. Y. Jeong, J. H. Lee, T. Nishimura, S. S. Lee, S. K. Kwak, Y. You and J. H. Jung, Circularly polarized luminescence active supramolecular nanotubes based on Pt^{II} complexes that undergo dynamic morphological transformation and helicity inversion, *Angew. Chem., Int. Ed.*, 2022, **61**, e202207310.
13 C. Ren, W. Sun, T. Zhao, C. Li, C. Jiang and P. Duan, A single-enantiomer emitter enabled superstructural helix inversion for upconverting and downshifting luminescence with bidirectional circular polarization, *Angew. Chem., Int. Ed.*, 2023, **62**, e202315136.
14 Y. Z. Ke, Y. Nagata, T. Yamada and M. Suginome, Majority-rules-type helical poly(quinoxaline-2,3-diyl)s as highly efficient chirality-amplification systems for asymmetric catalysis, *Angew. Chem., Int. Ed.*, 2015, **54**, 9333–9337.
15 M. Suginome, T. Yamamoto, Y. Nagata, T. Yamada and Y. Akai, Catalytic asymmetric synthesis using chirality-switchable helical polymer as a chiral ligand, *Pure Appl. Chem.*, 2012, **84**, 1759–1769.
16 M. Kumar, P. Brocorens, C. Tonnelé, D. Beljonne, M. Surin and S. J. George, A dynamic supramolecular polymer with stimuli-responsive handedness for in situ probing of enzymatic ATP hydrolysis, *Nat. Commun.*, 2014, **5**, 5793.
17 T. Kawasaki, M. Sato, S. Ishiguro, T. Saito, Y. Morishita, I. Sato, H. Nishino, Y. Inoue and K. Soai, Enantioselective synthesis of near enantiopure compound by asymmetric autocatalysis triggered by asymmetric photolysis with circularly polarized light, *J. Am. Chem. Soc.*, 2005, **127**, 3274–3275.
18 S. Shuvaev, M. A. Fox and D. Parker, Monitoring of the ADP/ATP ratio by induced circularly polarised europium luminescence, *Angew. Chem., Int. Ed.*, 2018, **57**, 7488–7492.
19 H. Kawamura, Y. Takeyama, M. Yamamoto, H. Kurihara, K. Morino and E. Yashima, Chirality responsive helical poly(phenylacetylene) bearing L-Proline pendants, *Chirality*, 2011, **23**, E35–E42.
20 N. Ousaka, Y. Takeyama and E. Yashima, Dinuclear metal complexes composed of peptide chains: solvent-induced switching and inversion of the metal-centered chirality, *Chem. Sci.*, 2012, **3**, 466–469.
21 A.-C. Chamayou, G. Makhloufi, L. A. Nafie, C. Janiak and S. Lüdeke, Solvation-induced helicity inversion of pseudo-tetrahedral chiral copper(II) complexes, *Inorg. Chem.*, 2015, **54**, 2193–2203.
22 A. Martinez, L. Guy and J.-P. Dutasta, Reversible, Solvent-induced chirality switch in atrane structure: control of the unidirectional motion of the molecular propeller, *J. Am. Chem. Soc.*, 2010, **132**, 16733–16734.
23 R. Lin, H. Zhang, S. Li, L. Chen, W. Zhang, T. B. Wen, H. Zhang and H. Xia, pH-Switchable inversion of the metal-centered chirality of metallabenzenes: opposite stereodynamics in reactions of ruthenabenzene with L- and D-cysteine, *Chem. – Eur. J.*, 2011, **17**, 2420–2427.
24 J. Gregoliński, M. Hikita, T. Sakamoto, H. Sugimoto, H. Tsukube and H. Miyake, Redox-triggered helicity inversion in chiral cobalt complexes in combination with H^+ and NO_3^- stimuli, *Inorg. Chem.*, 2016, **55**, 633–643.
25 L. Feng, Y. Wang and J. Jia, Triplet ground-state-bridged photochemical process: understanding the photoinduced chiral inversion at the metal center of $[Ru(phen)_2(L\text{-}ser)]^+$ and its bipy analogues, *Inorg. Chem.*, 2017, **56**, 14467–14476.

26 M. Rancan, J. Tessarolo, A. Carlotto, S. Carlotto, M. Rando, L. Barchi, E. Bolognesi, R. Seraglia, G. Bottaro, M. Casarin, G. H. Clever and L. Armelao, Adaptive helicity and chiral recognition in bright europium quadruple-stranded helicates induced by host-guest interaction, *Cell Rep. Phys. Sci.*, 2022, **3**, 100692.
27 S.-J. Hu, X.-Q. Guo, L.-P. Zhou, D.-N. Yan, P.-M. Cheng, L.-X. Cai, X.-Z. Li and Q.-F. Sun, Guest-driven self-assembly and chiral induction of photofunctional lanthanide tetrahedral cages, *J. Am. Chem. Soc.*, 2022, **144**, 4244–4253.
28 H. Miyake, H. Sugimoto, H. Tamiaki and H. Tsukube, Dynamic helicity inversion in an octahedral cobalt(II) complex system *via* solvato-diastereomerism, *Chem. Commun.*, 2005, 4291–4293.
29 D.-R. Ahn, T. W. Kim and J.-I. Hong, Induction of diastereoselectivity in Fe(II) tris(amino acid-bipyridine) complexes, *J. Org. Chem.*, 2001, **66**, 5008–5011.
30 H. Miyake, K. Yoshida, H. Sugimoto and H. Tsukube, Dynamic helicity inversion by achiral anion stimulus in synthetic labile cobalt(II) complex, *J. Am. Chem. Soc.*, 2004, **126**, 6524–6525.
31 S. Akine, S. Sairenji, T. Taniguchi and T. Nabeshima, Stepwise helicity inversions by multisequential metal exchange, *J. Am. Chem. Soc.*, 2013, **135**, 12948–12951.
32 S. Zahn and J. W. Canary, Electron-induced inversion of helical chirality in copper complexes of *N*,*N*-dialkylmethionines, *Science*, 2000, **288**, 1404–1407.
33 W. Xue, T. K. Ronson, Z. Lu and J. R. Nitschke, Solvent drives switching between Λ and Δ metal center stereochemistry of M_8L_6 cubic cages, *J. Am. Chem. Soc.*, 2022, **144**, 6136–6142.
34 T. Nabeshima, A. Hashiguchi, T. Saiki and S. Akine, Transfer of chiral information through achiral ion recognition by a novel pseudocrown ether with a binaphthyl moiety, *Angew. Chem., Int. Ed.*, 2002, **41**, 481–484.
35 M. Tsurui, R. Takizawa, Y. Kitagawa, M. Wang, M. Kobayashi, T. Taketsugu and Y. Hasegawa, Chiral tetrakis Eu(III) complexes with ammonium cations for improved circularly polarized luminescence, *Angew. Chem., Int. Ed.*, 2024, **63**, e202405584.
36 L. Arrico, C. De Rosa, L. Di Bari, A. Melchior and F. Piccinelli, Effect of the counterion on circularly polarized luminescence of europium(III) and samarium(III) complexes, *Inorg. Chem.*, 2020, **59**, 5050–5062.
37 J. Gregoliński, K. Ślepokura and J. Lisowski, Lanthanide complexes of the chiral hexaaza macrocycle and its meso-type isomer: solvent-controlled helicity inversion, *Inorg. Chem.*, 2007, **46**, 7923–7934.
38 S. Wada, Y. Kitagawa, T. Nakanishi, M. Gon, K. Tanaka, K. Fushimi, Y. Chujo and Y. Hasegawa, Electronic chirality inversion of lanthanide complex induced by achiral molecules, *Sci. Rep.*, 2018, **8**, 16395.
39 A. Gerus, K. Ślepokura and J. Lisowski, Anion and solvent induced chirality inversion in macrocyclic lanthanide complexes, *Inorg. Chem.*, 2013, **52**, 12450–12460.
40 S. Yin, X. Li, H. Wang, J. Li, W. Huang, T. Gao, P. Yan, Y. Zhou and H. Li, Coordination-driven self-assembly of a sandwich shaped Eu(III) complex for induced circularly polarized luminescence, *CrystEngComm*, 2023, **25**, 1541–1549.
41 D. G. Smith, R. Pal and D. Parker, Measuring equilibrium bicarbonate concentrations directly in cellular mitochondria and in human serum using europium/terbium emission intensity ratios, *Chem. – Eur. J.*, 2012, **18**, 11604–11613.
42 Y. Wang, Y. Zhou, Z. Yao, W. Huang, T. Gao, P. Yan and H. Li, Asymmetric induction in quadruple-stranded europium(III) helicates and circularly polarized luminescence, *Dalton Trans.*, 2022, **51**, 10973–10982.
43 S. Akine, S. Hotate and T. Nabeshima, A molecular leverage for helicity control and helix inversion, *J. Am. Chem. Soc.*, 2011, **133**, 13868–13871.
44 S. Sairenji, S. Akine and T. Nabeshima, Response speed control of helicity inversion based on a "regulatory enzyme"-like strategy, *Sci. Rep.*, 2018, **8**, 137.
45 Y. Okayasu, K. Wakabayashi and J. Yuasa, Anion-driven circularly polarized luminescence inversion of unsymmetrical europium(III) complexes for target identifiable sensing, *Inorg. Chem.*, 2022, **61**, 15108–15115.
46 W. Li, Y. Zhou, T. Gao, J. Li, S. Yin, W. Huang, Y. Li, Q. Ma, Z. Yao, P. Yan and H. Li, Circularly polarized luminescent $Eu_4(L^R)_4$ cage for enantiomeric excess and concentration simultaneous determination of chiral diamines, *ACS Appl. Mater. Interfaces*, 2022, **14**, 55979–55988.
47 C. P. Montgomery, E. J. New, D. Parker and R. D. Peacock, Enantioselective regulation of a metal complex in reversible binding to serum albumin: dynamic helicity inversion signalled by circularly polarised luminescence, *Chem. Commun.*, 2008, 4261–4263.
48 Y. Kono, N. Hara, M. Shizuma, M. Fujiki and Y. Imai, Complexes of Eu(III)$(hfa)_3$ with a planar chiral P(III) ligand (phanephos): solvent-sensitive sign inversion of circularly polarised luminescence, *Dalton Trans.*, 2017, **46**, 5170–5174.
49 J. Yuasa, H. Ueno and T. Kawai, Sign reversal of a large circularly polarized luminescence signal by the twisting motion of a bidentate ligand, *Chem. – Eur. J.*, 2014, **20**, 8621–8627.
50 T. Y. Bing, T. Kawai and J. Yuasa, Ligand-to-ligand interactions that direct formation of D_2-symmetrical alternating circular helicate, *J. Am. Chem. Soc.*, 2018, **140**, 3683–3689.
51 S. G. Telfer, T. M. McLean and M. R. Waterland, Exciton coupling in coordination compounds, *Dalton Trans.*, 2011, **40**, 3097–3108.
52 J. L. Lunkley, D. Shirotani, K. Yamanari, S. Kaizaki and G. Muller, Chiroptical spectra of a series of tetrakis((+)-3-heptafluorobutylyrylcamphorato)lanthanide(III) with an encapsulated alkali metal ion: circularly polarized luminescence and absolute chiral structures for the Eu(III) and Sm(III) complexes, *Inorg. Chem.*, 2011, **50**, 12724–12732.
53 Y. Zhou, H. Li, T. Zhu, T. Gao and P. Yan, A highly luminescent chiral tetrahedral $Eu_4L_4(L')_4$ cage: chirality induction, chirality memory, and circularly polarized luminescence, *J. Am. Chem. Soc.*, 2019, **141**, 19634–19643.

54 Y. B. Tan, Y. Okayasu, S. Katao, Y. Nishikawa, F. Asanoma, M. Yamada, J. Yuasa and T. Kawai, Visible circularly polarized luminescence of octanuclear circular Eu(III) helicate, *J. Am. Chem. Soc.*, 2020, **142**, 17653–17661.
55 K. Takaishi, K. Iwachido and T. Ema, Solvent-induced sign inversion of circularly polarized luminescence: control of excimer chirality by hydrogen bonding, *J. Am. Chem. Soc.*, 2020, **142**, 1774–1779.
56 M. Bogojeski, L. Vogt-Maranto, M. E. Tuckerman, K.-R. Müller and K. Burke, Quantum chemical accuracy from density functional approximations via machine learning, *Nat. Commun.*, 2020, **11**, 5223.
57 T. Lu and F. Chen, Multiwfn: a multifunctional wavefunction analyzer, *J. Comput. Chem.*, 2012, **33**, 580–592.
58 C. Lefebvre, G. Rubez, H. Khartabil, J.-C. Boisson, J. Contreras-García and E. Hénon, Accurately extracting the signature of intermolecular interactions present in the NCI plot of the reduced density gradient versus electron density, *Phys. Chem. Chem. Phys.*, 2017, **19**, 17928–17936.
59 T. Lu and Q. Chen, Independent gradient model based on Hirshfeld partition: a new method for visual study of interactions in chemical systems, *J. Comput. Chem.*, 2022, **43**, 539–555.